Volume 50 | Number 42 | 30 May 2014 | Pages 5519–5666

ChemComm

Chemical Communications

www.rsc.org/chemcomm

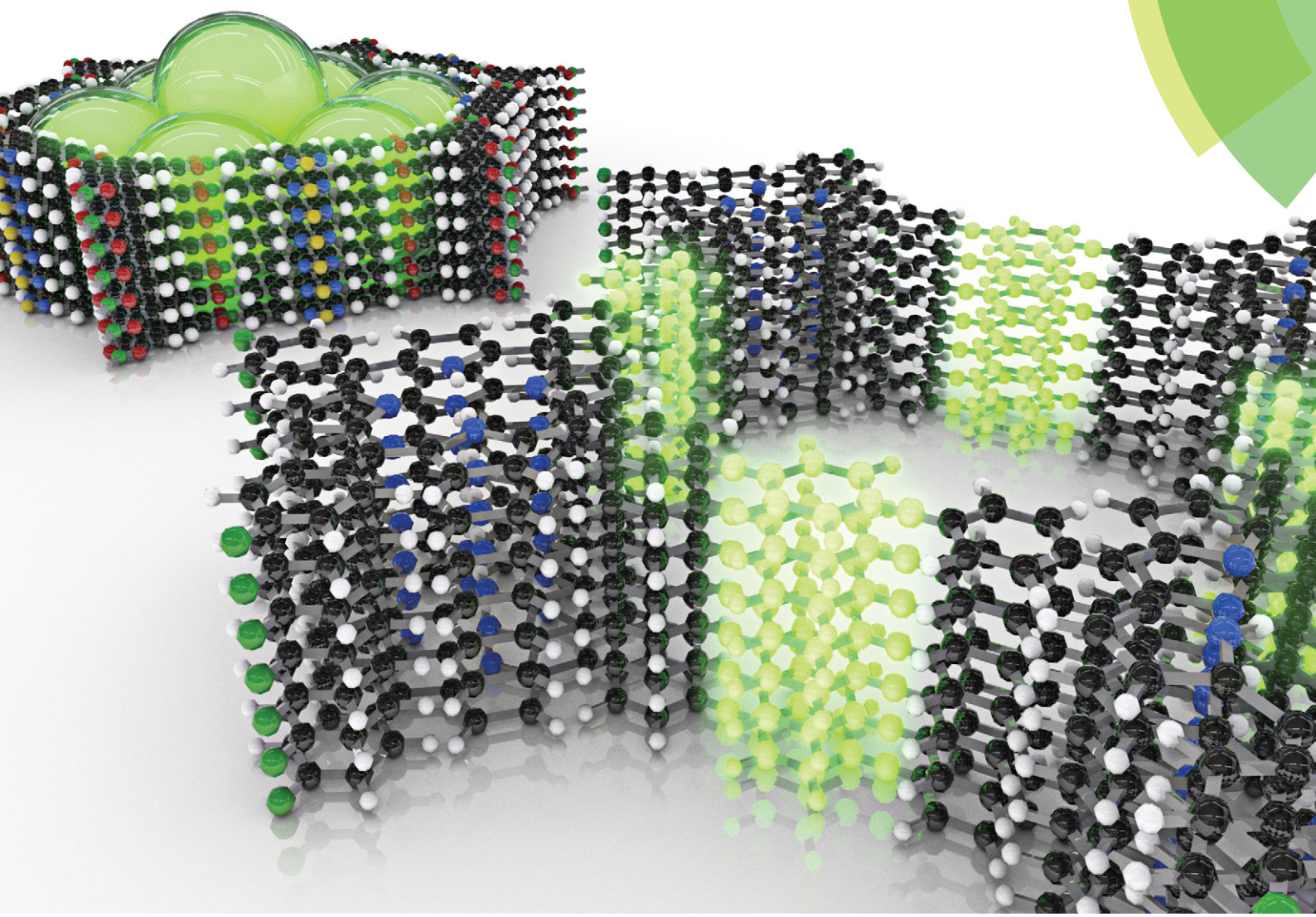

ISSN 1359-7345

ROYAL SOCIETY OF CHEMISTRY

FEATURE ARTICLE

Mirjam Dogru and Thomas Bein

On the road towards electroactive covalent organic frameworks

ChemComm

FEATURE ARTICLE

View Article Online
View Journal | View Issue

On the road towards electroactive covalent organic frameworks

Cite this: *Chem. Commun.*, 2014, **50**, 5531

Mirjam Dogru and Thomas Bein*

Received 4th September 2013,
Accepted 20th November 2013

DOI: 10.1039/c3cc46767h

www.rsc.org/chemcomm

Covalent organic frameworks (COFs) are a novel class of porous crystalline organic materials assembled from molecular building blocks. The construction principles of these materials allow for the design of precisely controllable structures since their chemical and physical properties can be easily tuned through the selection of the building blocks and the linkage motif. Their extraordinary and versatile properties impart functionality that is of great interest in areas such as gas storage, separation, catalysis and optoelectronics. This feature article discusses key aspects of the design of covalent organic frameworks with a focus on electroactive COFs for potential optoelectronic and photovoltaic applications.

Introduction

Ordered porous materials have attracted enormous attention due to their exceptional properties and their numerous existing and potential applications.[1–7] Focussing on nanoporous materials, during the last few decades an increasing degree of structural control was achieved to precisely match the properties of these materials with their intended applications. Tailoring the metrics, composition, as well as chemical and physical properties of these nanostructures can now be achieved for an increasing number of materials by designing reactants such as building blocks and templating agents or reaction conditions.

Nanoporous frameworks such as zeolites, aluminophosphates (AlPOs) or metal–organic frameworks (MOFs) are attractive due to their well-defined crystalline nature combined with a great structural and compositional variety. Crystallinity implies atomically precise definition of pore sizes, pore shapes, pore topology, and internal distribution of reactive sites, just to name a few. Thus, storage, separation and catalytic conversion of molecules are among the most prominent applications of these materials. For many concepts addressing efficient energy storage or energy conversion, accessible high internal surfaces with well-defined and tunable wall properties are often desirable for charge transfer and transport. Global warming and the need for a sustainable energy supply illustrate the importance of discovering and developing new materials and technologies in the field of clean or renewable energy, including gas storage, photocatalysis or photovoltaics. For example, solar cells have great potential as emission-free energy sources, however this technology is still too expensive to compete with fossil fuel-based power.[8] In this context, the extensively investigated field of organic semiconductors provides several attractive features with respect to conventional inorganic solar cells. Many organic compounds can be efficiently produced and processed on a large scale and can be easily modified by the versatile tools of organic chemistry.[9,10] The ability to design the desired material on a molecular basis permits fine tuning of the energy gap and the light absorbance of the semiconductor. In addition, due to large absorption coefficients even small amounts of the photoactive species offer the potential for efficient energy conversion. This allows for the fabrication of very thin devices. However, important issues still need to be addressed, for example, the devices often exhibit low stability and efficiencies that are lower than expected. The latter is often caused by low charge carrier mobilities and recombination, due to inefficient stacking of the conducting polymers or due to insufficient and disordered donor–acceptor interfaces. Therefore it would be desirable to have synthetic access to conducting materials with total control over their nanoscale structure and orientation.

Organic photovoltaics – design principles

Organic photovoltaics have promising potential as emission free and sustainable energy sources. However, several challenges including limited efficiency and device stability still need to be overcome. Over the years several design strategies were developed to address these issues. Key criteria for higher efficiency in organic solar cells are a high absorbance, fast diffusion of excitons (strongly bound electrons and holes), efficient charge separation and transfer at the donor–acceptor interface, and efficient charge collection. In the following we briefly summarize the developed design principles regarding the structure of the active layer in organic solar cell devices.

Department of Chemistry and Center for NanoScience (CeNS), University of Munich (LMU), Butenandtstr. 5-13 (E), 81377 Munich, Germany. E-mail: bein@lmu.de; Fax: +49-(0)89-2180-77622; Tel: +49-(0)89-2180-77621

The first donor–acceptor system (D–A system), a bilayer planar heterojunction, was introduced by Tang in 1979.[11] The concept of combining a donor and acceptor layer revolutionized the field of organic solar cells and paved the way towards creating more efficient donor–acceptor architectures. The first 1% solar cell was achieved by Tang with a system that contained a derivative of phthalocyanine as donor material and a perylene derivative serving as acceptor material. The main advantage of a D–A-system is the enhanced charge separation compared to a single layer device.[8] The introduction of C_{60} fullerene and its derivatives, such as [6,6]-phenyl C_{61} butyric acid methyl ester ([60]PCBM),[12] as acceptor molecules helped to enhance efficiency. The most intensively studied systems today are polymer–fullerene combinations. In 1992 the first electron transfer between a fullerene and a polymer was independently demonstrated by Heeger *et al.* and Yoshino *et al.*[13,14] Only one year later the first polymer–fullerene photovoltaic device was reported.[15] A major breakthrough towards higher efficiencies was realized by mixing the donor and acceptor phases to form interpenetrated donor–acceptor systems; these so-called bulk heterojunctions were introduced by Hiramoto *et al.* through the co-evaporation of donor and acceptor molecules under high-vacuum conditions. The first organic photovoltaic devices based on mixed phases of polymer–fullerene and polymer–polymer were independently reported by Heeger and Friend.[16,17] The widely postulated ideal structure for an efficient organic solar cell is a bicontinuous and interpenetrated network of the donor and acceptor phases in a bulk heterojunction (Fig. 1).[10]

In these bulk heterojunctions the active layer forms a diffuse interface between the donor and acceptor, thus the interface is significantly larger and more charges can be separated at the donor acceptor interface, compared to planar bilayers. The overall efficiency for exciton dissociation could be improved and long exciton lifetimes in the bulk materials were no longer necessary. However, we note that for efficient charge transport and collection of photogenerated electrons and holes efficient percolation pathways are required. Clearly, the percolation pathways will strongly depend on the morphology of each semiconductor phase.[18,19] Numerous studies show how the morphology of the donor–acceptor blends can be influenced, the most exhaustively studied D–A systems being poly(3-hexylthiophene) (P3HT) and [6,6]-phenyl C_{61} butyric acid methyl ester ([60]PCBM). It was demonstrated that the performance of the active layer is extremely sensitive towards synthesis parameters, such as the ratio of the polymer to fullerene, solvent or solvent mixtures, additives, and thermal or solvent annealing.[20–23] However, while in donor–acceptor blends the (disordered) morphology of both materials can be influenced to a certain degree, it cannot be predicted and control over the structural parameters is lacking. In the following, different concepts aimed at controlling the morphology of the active layer at the nano or even atomic scale will be discussed. The first attempt was to covalently attach the acceptor fullerene moieties to the donor polymer backbone (Fig. 2a). The first so-called double cable polymers with a polythiophene backbone were reported in 1996 by Benincori *et al.*[24] and one year later by Yassar *et al.*[25] These compounds were intensively investigated in organic photovoltaics, however, until now only rather low efficiencies could be reported.[26–28] This was attributed to increased recombination, due to too short distances between the donor and acceptor on the one hand and non-ideal packing and low concentration of fullerene on the other hand. Increasing the amount of fullerene and the distance between D and A was expected to lead to higher efficiencies. It became obvious that the domain size and morphology of donor and acceptor phases at the nanoscale are crucial for the device performance. Generally, using self-assembly processes of di-block copolymers can permit morphological control of the donor–acceptor phases on the nanometer scale.[29,30] The concept of using diblock copolymers in organic solar cells was presented by Sun *et al.*[31] The resulting structures can be fine-tuned by changing synthetic parameters, the domain size and the phase separation behavior can be adjusted by choosing the type of the copolymer, and the overall nano-morphology can be shaped by the volume fraction of the components (Fig. 2b).[32,33] With these systems the elusive goal of elucidating the direct impact of nano-morphology on the photovoltaic efficiency seemed to be within reach. However, while the resulting D–A interfaces served well to separate charges (as shown by efficient luminescence quenching) unfortunately these systems faced severe recombination losses and low efficiencies.[34–36] It was postulated that recombination might be reduced by inserting spacers between the donor and acceptor branches of the polymer.[37] Furthermore control over the orientation relative to the substrate was also viewed as a way to increase the efficiency.[37] Another approach was introduced by Müllen and co-workers, relying on a self-assembly process induced by differences in solubility of hexabenzocoronene and perylenebisdicarboximide (Fig. 2c). The donor and acceptor phases assemble into a bilayered structure with large interfacial area.[38] In addition to 'bottom up' strategies based on molecular assembly, 'top down' methods were also developed with a view of creating ordered nanomorphologies for photovoltaics. For example, nanoimprint lithography is capable of creating interpenetrated organic photovoltaic devices (Fig. 2d). Thereby a pattern is imprinted from a mold onto a substrate

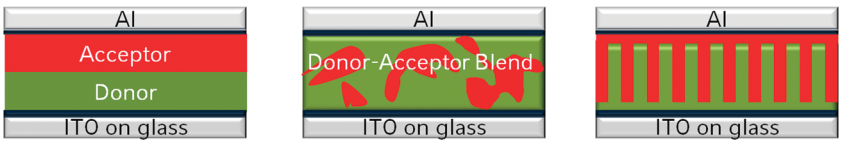

Fig. 1 Evolution of the organic solar cell devices from bilayer to blended bulk heterojunctions and targeted ordered interpenetrated donor–acceptor systems.

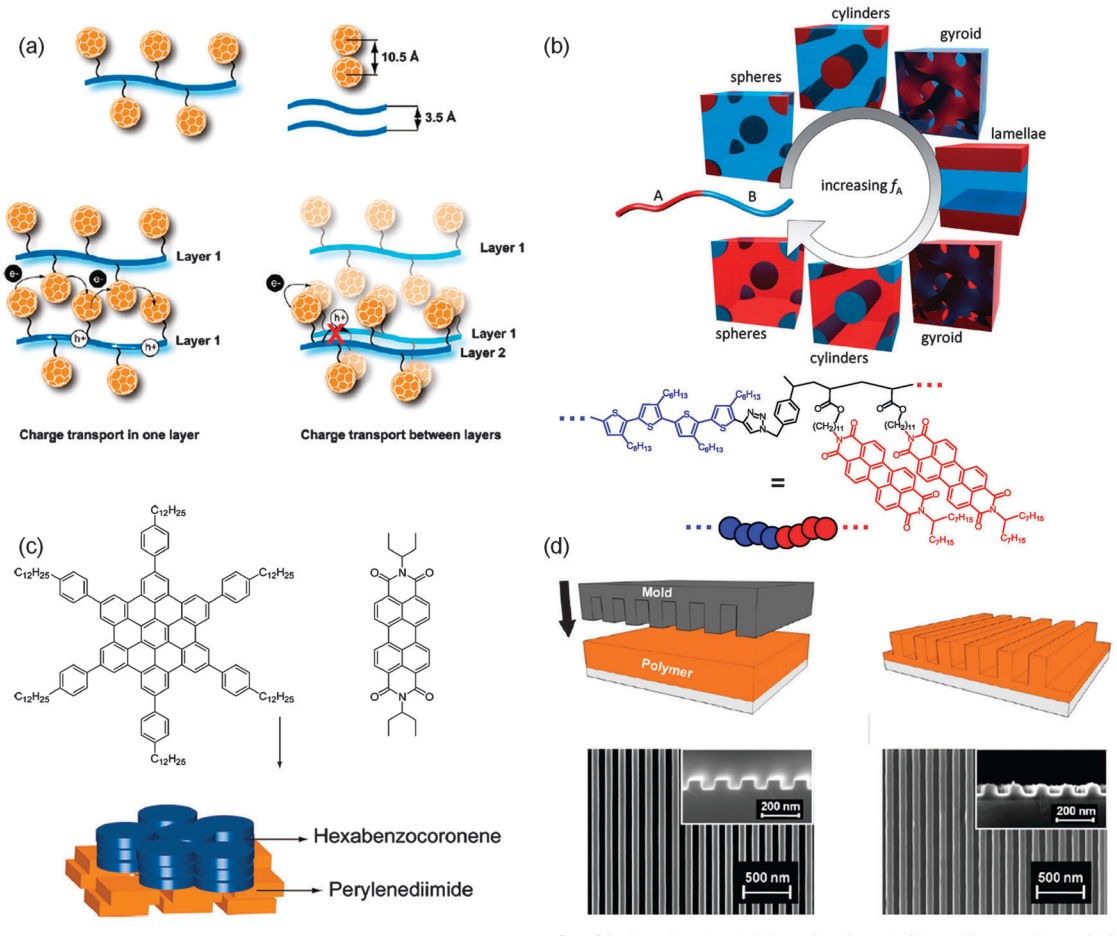

Fig. 2 Examples of ordered organic donor–acceptor systems. (a) Illustration of double cable polymers, adapted with permission from ref. 33, copyright 2010 American Chemical Society, (b) di-block copolymer morphologies as a function of molar fraction and schematic representation of a di-block copolymer, reproduced from ref. 40; (c) self-assembly of hexabenzocoronene and perylenediimide, adapted with permission from ref. 33, copyright 2010 American Chemical Society, (d) nanoimprint process flow, mold pressed onto a polymer and SEM images of (left) Si nanolined mold and (right) nanoimprinted P3HT, adapted with permission from ref. 39, copyright 2012 American Chemical Society.

that is coated with an organic film; the structure of the mold determines the structure of the film. The complimentary semiconductor can be deposited on the imprinted film by spin coating a solution. Hereby the penetration of the solution into the nanostructured film is crucial to obtain an intimate contact and a large-area donor acceptor interface.[39]

In addition to organic and inorganic solar cells, hybrid organic–inorganic systems have also attracted much attention. Typical hybrid solar cells comprise nanostructures (*e.g.*, arrays of nanorods or nanotubes) of zinc oxide, titanium oxide or cadmium selenide that function as acceptors for interpenetrating polymer donors.[37,41,42] While such designs often take advantage of inorganic solid nanostructures to control nanomorphologies to a certain degree, they are not within the scope of this review.

In this review we will explore the potential of a new class of materials, covalent organic frameworks (COFs), as promising candidates for organic solar cells. Based on the powerful toolbox of organic chemistry, these crystalline systems are proposed as an intriguing family of highly defined model systems that provide the possibility to investigate the impact of nanomorphology on the behavior of photovoltaic systems in great detail. After a short introduction to this new class of materials we will focus on electroactive covalent organic frameworks and their potential in organic solar cells.

Covalent organic frameworks

Covalent organic frameworks, first reported in 2005 by Yaghi *et al.*, are organic, crystalline and highly porous materials constructed from light elements such as hydrogen, boron, carbon, nitrogen and oxygen. The COF frameworks consist of organic building blocks connected by covalent bonds, the slightly reversible nature of their bonding motifs being favorable for the generation of self-assembled 2D or 3D framework structures. Yaghi's group initially created ordered crystalline networks by making use of a reversible boronate ester condensation.[43,44] This type of chemistry has led to the design and synthesis of many new porous materials whose composition, structure, metrics and functionality can be systematically varied.

Their extraordinary features including high surface areas, molecular control of the internal surface and thermal stability in combination with semiconducting properties make them intriguing candidates for gas storage, catalysis and optoelectronics.

1.1. Synthesis principles

First structures. Crystalline COFs containing 2D-layers were synthesized in one-step condensation reactions of organic building blocks resulting in either hexagonal or tetragonal layers depending on the geometry and connectivity of the linkers. These two-dimensional layered structures are held together by π-stacking in the third dimension. This leads to pores accessible in one direction. The synthesis of COF-1, the first COF introduced by Yaghi in 2005, is based on the dehydration reaction of 1,4-benzenediboronic acid (BDBA).[43] The condensation of the diboronic acid leads to the formation of a planar six-membered ring of B_3O_3 (boroxine) accompanied by the elimination of three water molecules (Fig. 3).[45] The formation of the network is entropically favoured due to liberation of water molecules. Planar 2D organic sheets are formed, which are stacked in a staggered arrangement.

Yaghi postulated that the reaction has to be carried out in a closed reaction system with solvents in which diboronic acid is not completely soluble. These conditions allow a slow condensation of BDBA. The sparing solubility of BDBA in this system controls the diffusion of the building blocks into solution and facilitates the nucleation of a crystalline material. The use of a closed reaction system sustains the availability of H_2O for maintaining slightly reversible conditions conducive to crystallite growth.[43] The co-condensation reaction of diboronic acid with the trigonal building block hexahydroxytriphenylene (HHTP) produces a five-membered BO_2C_2 ring (Fig. 3). In order to build up a 2D COF the organic linkers have to meet certain criteria. Connectivity of the organic building blocks is one criterion. Until now organic building block combinations with either linear–trigonal, trigonal–trigonal or linear–tetragonal connectivity gave a large variety of COF structures.[4,5]

In 2006 Lavigne reported a reverse assembly concept, *i.e.* co-condensation of a linear alcohol (tetraol) with a triangular triboronic acid giving COF-18 Å.[46] In 2007 Yaghi and co-workers extended the scope of 2D hexagonal COFs. COF-6, -8 and 10 were synthesized by linking the trigonal HHTP with trigonal 1,3,5-benzenetriboronic acid (BTBA), trigonal 1,3,5-benzenetris(4-phenylboronic acid) (BTPA) or linear 4,4′-biphenyldiboronic acid (BPDA), respectively.[47] Due to the reticular assembly of planar aromatic building blocks of different size, COFs with varying pore sizes from 0.9 to 4.7 nm were constructed.

For host–guest interactions with large molecules, pores with several nm in diameter are desired. Recently we introduced the BTP-COF with fully accessible open pores of 4 nm, synthesized by co-condensation of 1,3,5-benzenetris(4-phenylboronic acid) (BTPA) and the polyol 2,3,6,7-tetrahydroxy-9,10-dimethylanthracene (THDMA).[48] After degassing the material for 12 h at 150 °C a large surface area of 2000 $m^2\ g^{-1}$ was obtained; this value agrees well with the calculated Connolly surface. The largest pore size reported until now was achieved by condensing 2,3,6,7,10,11-hexahydroxytriphenylene (HHTP) and 4,4′-diphenylbutadiyne bis(boronic acid) (DPBA).[49] The porosity of the HTTP-DPB

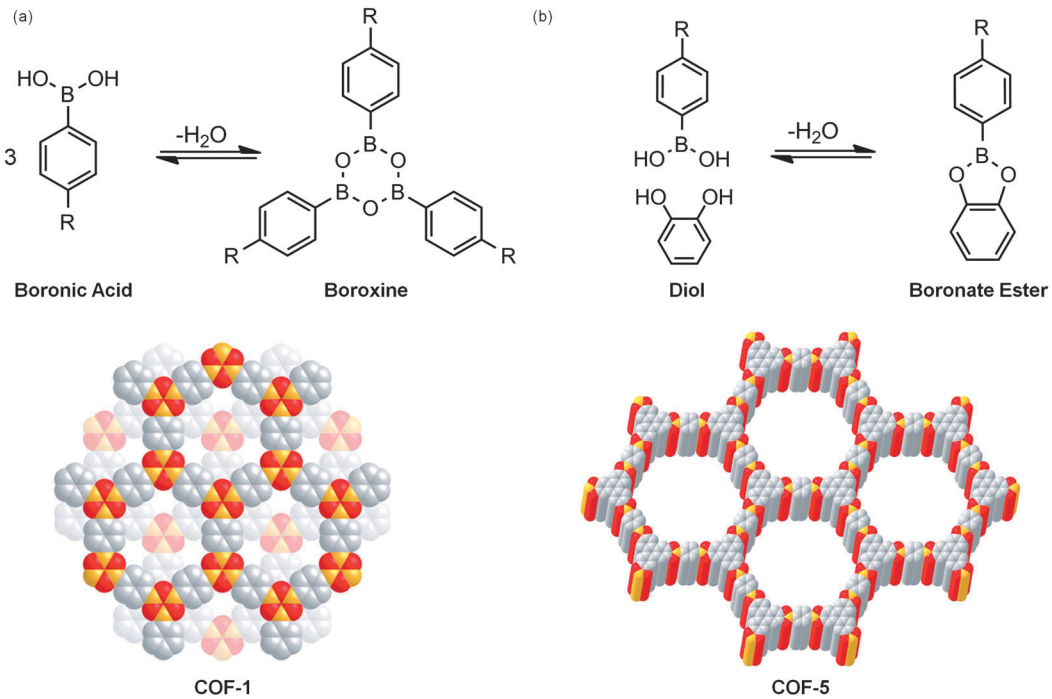

Fig. 3 Reversible reactions of boronic acids: (a) self-condensation forms a boroxine ring resulting in a staggered COF-1, and (b) co-condensation with a vicinal diol (HHTP) forms a boronate ester resulting in COF-5. Coloring scheme: C, gray; H, white, B, orange, O, red. Adapted with permission from ref. 43. Copyright 2005 AAAS.

COF was evaluated by nitrogen sorption measurements. The obtained BET surface of 930 $m^2\ g^{-1}$ was compared to a simulated isotherm using Monte Carlo simulations (2670 $m^2\ g^{-1}$) and to the calculated Connolly surface (2640 $m^2\ g^{-1}$), thus achieving access to about 40% of the theoretical porosity of the COF. The interlayer stacking of this material was evaluated by molecular dynamics and DFT calculations, predicting a offset of about 0.17 nm between the adjacent layers of the hexagonal sheets.

The first non-hexagonal 2D COF was reported by Spitler *et al.*, made by condensing a tetragonal octaol, or more precisely a tetragonal phthalocyanine tetra(acetonide) with a linear diboronic acid and addition of catalytic amounts of a Lewis acid (BF_3*OEt_2) to form a tetragonal lattice.[50] Following the concept of reticular chemistry, several tetragonal COF structures have been made to date, ranging from the microporous to the mesoporous regime with nominal pore sizes up to 4.4 nm.[51–55] The condensation of zinc porphyrin tetraboronic acid with tetrahydroxybenzene was investigated using different solvent ratios and reaction times. Due to the solubility of the porphyrin species in dioxane the solvent ratio had to be adjusted to a higher mesitylene content allowing a reversible self-healing and slow crystallization. After 15 days at 120 °C cube-shaped crystals sized about 0.5 μm were obtained.[52] In Fig. 4, building blocks with different connectivity and resulting COF structures are depicted.

Synthesis techniques. The above examples show the successful crystallization of hexagonal and tetragonal organic frameworks. The great variety of organic building blocks applicable as starting materials offers great potential to design new porous solids. While crystallization of bulk COFs under solvothermal synthesis conditions typically requires many hours, Campbell *et al.* reported a high-throughput microwave synthesis protocol that enables an acceleration of the reaction time by a factor of about 200.[56] Recently we reported a two-step microwave driven reaction for a benzothiadiazole-based covalent organic framework, BTD-COF, starting from a pinacol protected boronic ester instead of a free boronic acid. This allows for the incorporation

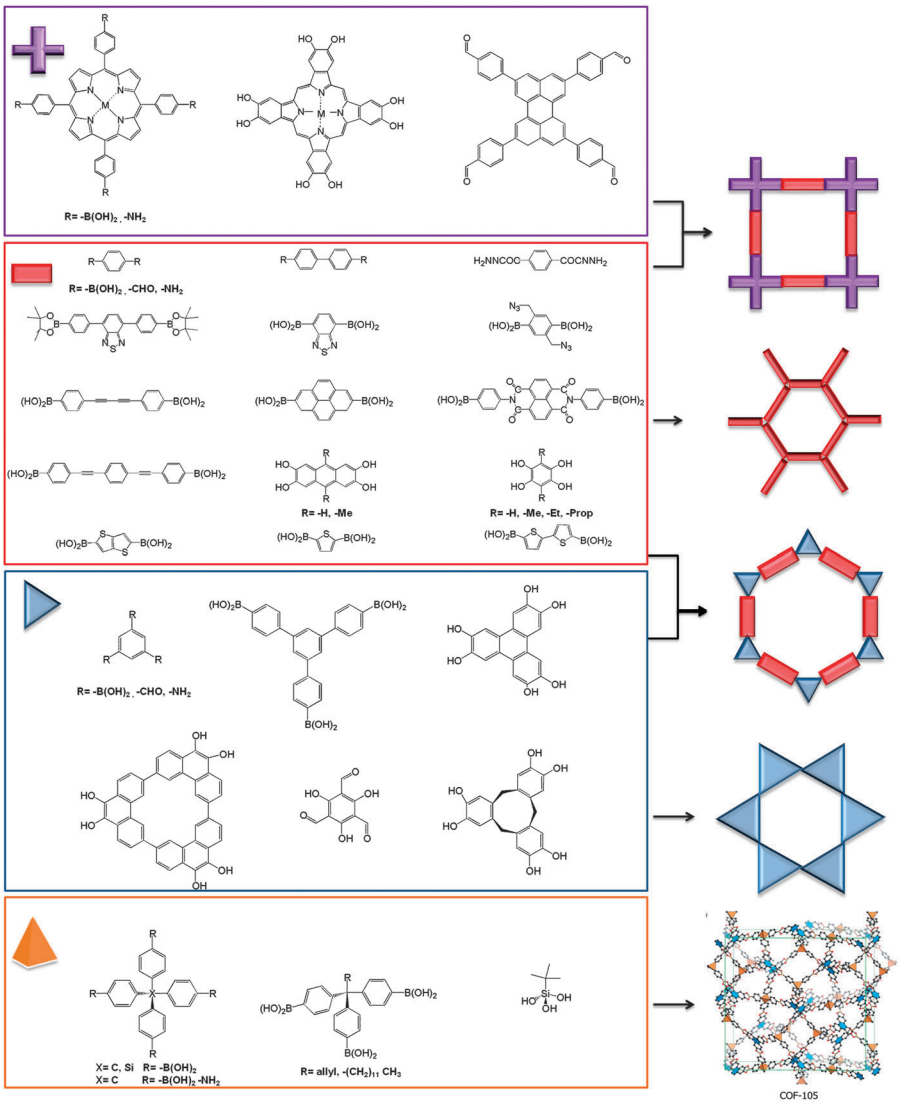

Fig. 4 Building blocks used for COF synthesis, categorized by their connectivity leading to tetragonal, hexagonal or 3D COFs.

of large poorly soluble aromatic building blocks, from which the free boronic acid is difficult to access. This way the formation of a mesoporous COF is possible in only 60 min.[57] Sonochemical treatment also enables reduced reaction times, resulting in the successful formation of COF-1 and COF-5 within 1 h.[58]

Banerjee and co-workers recently reported a new route to acid- and base-stable COFs using a combination of a reversible and an irreversible organic reaction. In the first step the COFs were synthesized by the reversible Schiff base reactions of 1,3,5-triformylphloroglucinol (Tp) with *p*-phenylenediamine (Pa-1) and 2,5-dimethyl-*p*-phenylenediamine (Pa-2), respectively. The expected enol–imine (OH) form underwent irreversible proton tautomerism, and only the keto–enamine form was obtained, which resists boiling water, strong acids and bases.[59] The formation of three isoreticular covalent organic frameworks (COFs) *via* a room-temperature and solvent-free mechanochemical synthesis route was recently reported by Biswal *et al.*[60] However, while such methods would allow for large-scale COF production, these mechanochemically synthesized COFs show rather poor crystallinity and porosity.

3D frameworks. In 2007 Yaghi extended the idea of linking organic building blocks by covalent bonds from two-dimensional structures to 3D frameworks. This was accomplished by linking tetrahedral and triangular building blocks together (Fig. 5). Tetra(4-dihydroxyborylphenyl)methane (TBPM), for example, reacts in a self-condensation reaction to form triangular B_3O_3 rings giving the so-called COF-102. The tetrahedral building block TBPM can also undergo a co-condensation reaction with HHTP forming C_2O_2B rings and resulting in the framework structure of COF-105. Using the silane-analog of TBPM, tetra(4-dihydroxyborylphenyl)silane (TBPS) in self- or co-condensation reactions gives COF-103 and COF-108, respectively.[44]

These structures are among the most porous frameworks, exhibiting fully accessible porosity with surface areas as high as 4210 $m^2\ g^{-1}$ (COF-103), comparable to the surface areas of MOFs such as MOF-177 (4500 $m^2\ g^{-1}$)[62] and MIL-101.[63] Furthermore, COF-108 is one of the most porous organic materials with the lowest density (0.17 g cm^{-3}) reported.[44] Therefore these materials are extensively investigated for gas storage applications. Expanding the idea of reticular chemistry, Hunt *et al.* employed the condensation of borosilicate clusters, known from the borosilicate glass Pyrex, to build thermally and chemically stable 3D COFs. COF-202 is formed by B–O–Si linkage of *tert*-butylsilane and the tetrahedral tetra(4-dihydroxyboryl-phenyl)-methane (Fig. 5). The *tert*-butyl groups are facing the pores of the network providing a chemically transformable site with sufficient space for further reactions.[61] While the gas storage properties of COFs are of great present interest, they are not within the scope of this review. The interested reader is referred to pertinent articles and reviews.[4,5,64–70]

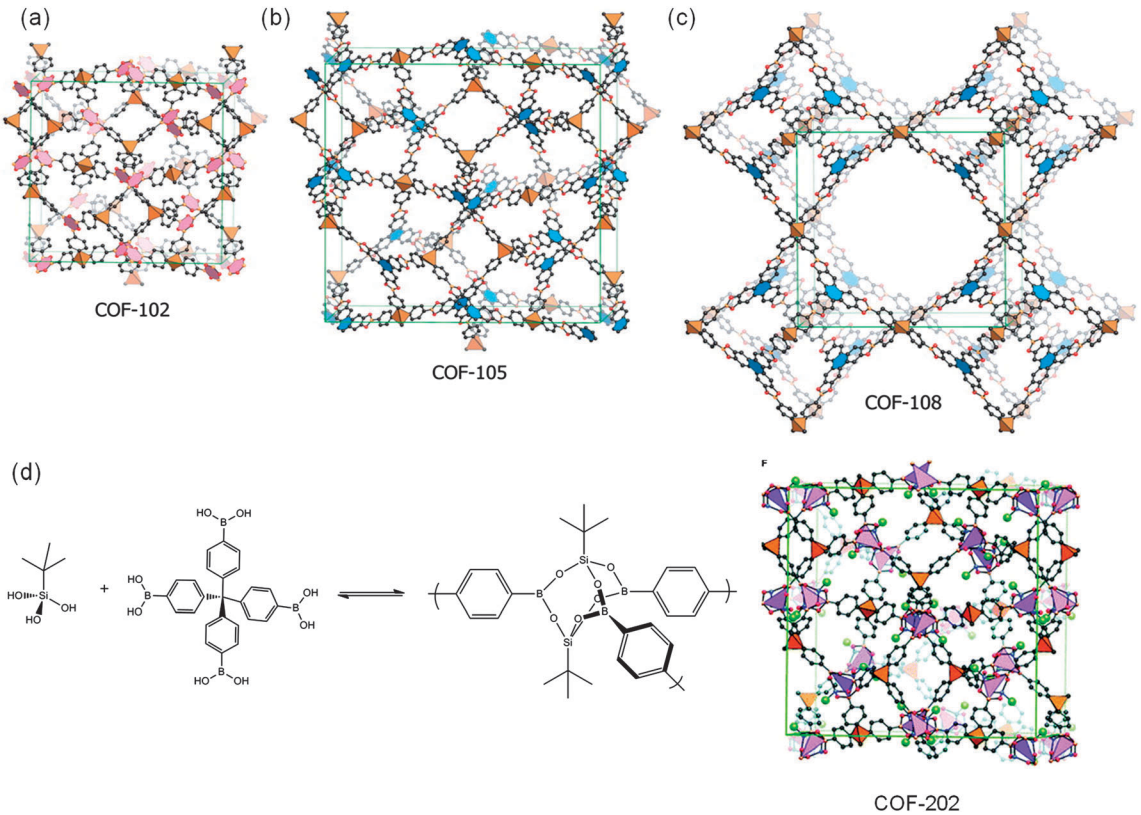

Fig. 5 Modeled crystalline structures of COF-102 (a), COF-105 (b), and COF-108 (c), reprinted with permission from ref. 44, copyright 2007 AAAS. Condensation of *tert*-butylsilane triol with tetra(4-dihydroxyboryl-phenyl)methane as boronic acid forms a borosilicate cage and gives a 3D crystalline framework with the crystalline structure depicted in (d). Color code: carbon is grey, boron is illustrated as orange and oxygen atoms are represented as red. Adapted with permission from ref. 61. Copyright 2008 American Chemical Society.

Linkage motifs. Recently Yaghi and co-workers further developed the linkage chemistry for COF synthesis. When reacting amines and aldehydes, imines are formed (Schiff base reaction). The first imine-linked 3D COF was produced by solvothermal synthesis of a tetrahedral tetra-(4-anilyl)methane and terephthalaldehyde resulting in a diamond topology.[71] A 2D COF, synthesized by Schiff base reaction of a tetraamino porphyrin and terephthalaldehyde was recently reported.[54] Ding *et al.* reported the first 2D imine linked COF, named COF-LZU1, with a pore size of about 1.8 nm.[72] Using pyrene-cores and linking them *via* imine formation, imine-based COFs were expanded into the mesoporous regime.[73] Moreover, using the dehydration reaction of 2,5-diethoxyterephthalohydrazide and 1,3,5-triformylbenzene or 1,3,5-tris(4-formylphenyl)benzene, hydrazone-linked COFs were successfully produced.[74] Jackson *et al.* reported the first crystalline borazine linked COF, namely BLP-2 (H). The borazine ring formation is achieved by a thermal decomposition reaction at 120 °C of 1,3,5-tris(*p*-aminophenyl)-benzene-borane in mesitylene and toluene.[75] Another group of covalently bonded organic frameworks was formed by a trimerization reaction of dicyanobenzene derivatives. Under ionothermal conditions at 400 °C in zinc chloride melt, the nitrile-based starting materials are soluble. Furthermore the triazine formation is reversible, enabling the crystallization of an ordered highly porous framework with high thermal stability. The resulting CTF-1, synthesized by the trimerization of 1,4-dicyanobenzene shows an XRD pattern similar to activated COF-1, to which it is isoelectronic. Furthermore, the surface area of 791 $m^2\ g^{-1}$ and pore volume of 0.40 $cm^3\ g^{-1}$ of CTF-1 are comparable to the values of COF-1 (711 $m^2\ g^{-1}$ and 0.32 $cm^3\ g^{-1}$). Important reversible linkage motifs are schematically shown in Fig. 6.[76]

Pore modification. Functionalization of the pore dimensions and the intra-pore environment can be realized by rational pre-selection of the organic linkers used for COF synthesis. Using such a pre-synthetic functionalization approach, the COF material can be customized for desired applications. For example, Tilford *et al.* illustrated micropore tailoring of COF-18 Å down from 1.8 nm to 1.1 nm.[77] For this purpose, tetrahydroxybenzene was modified with alkyl side chains of up to three carbon atoms. The authors showed that the incorporated alkyl substituents influence host–guest interactions. On the one hand nitrogen uptake is reduced, but on the other, the amount of adsorbed hydrogen into the framework increased substantially (Fig. 7a). The incorporation of a great variety of organic moieties *via* the pre-synthetic modification approach, however, is not straightforward. For the COF synthesis factors such as the compatibility of the anchoring group with reaction conditions (*e.g.* solvent, temperature) or the spatial extent of the

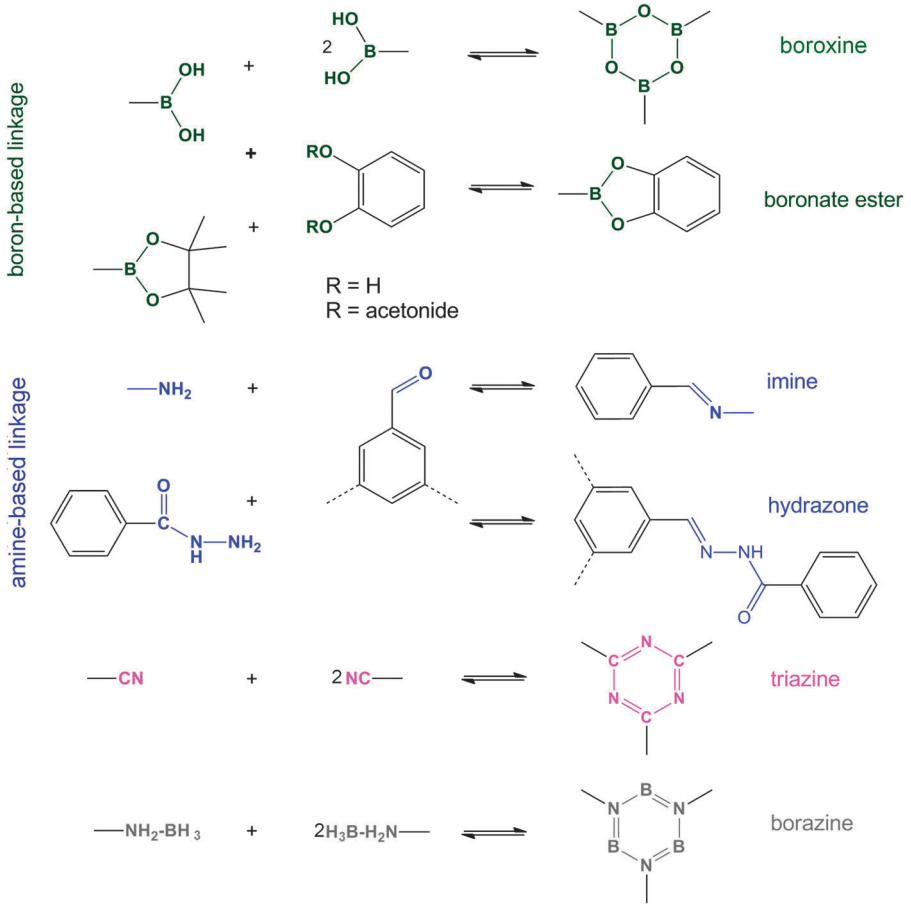

Fig. 6 Reversible reactions resulting in successful linkage motifs for COF synthesis.

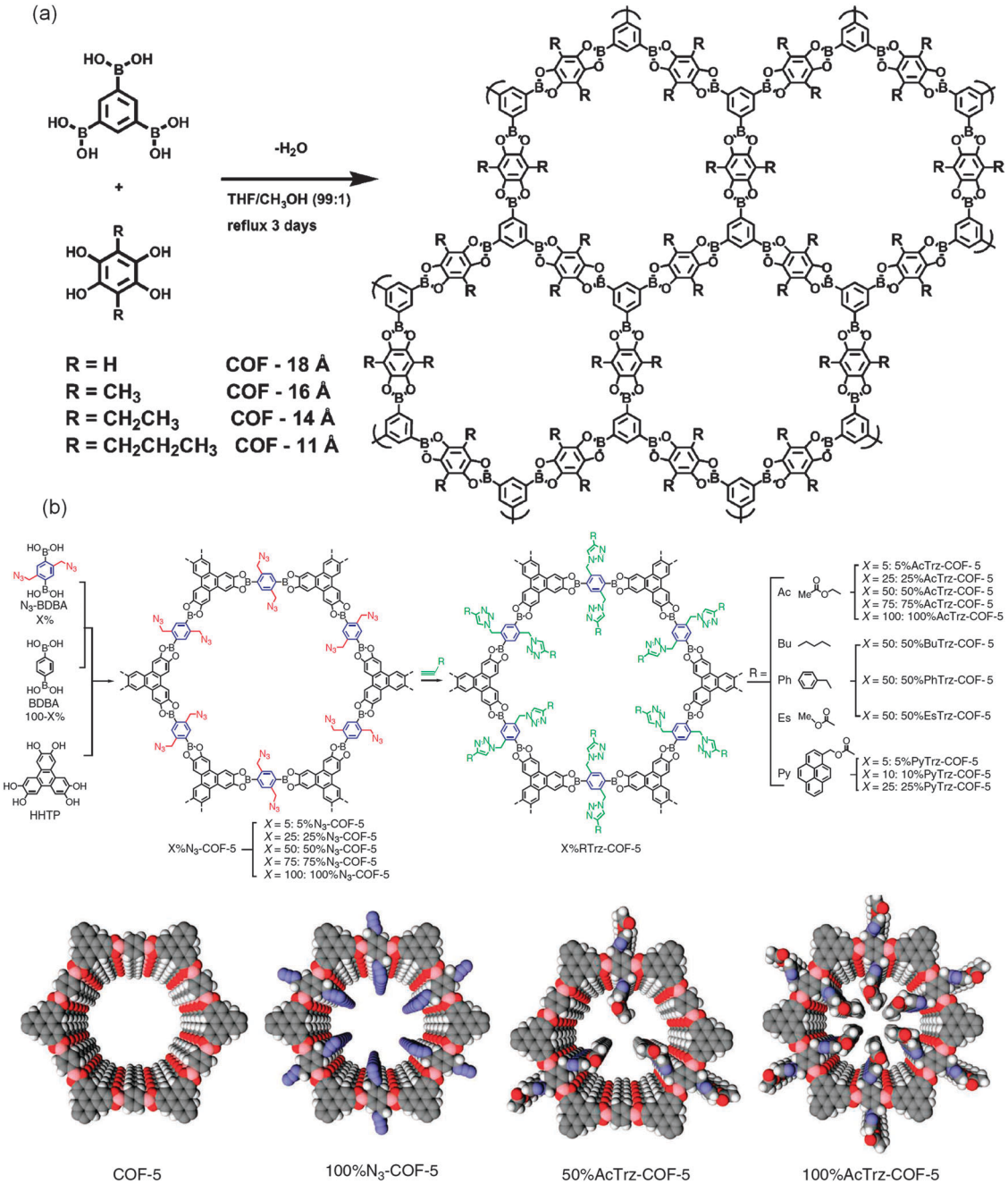

Fig. 7 (a) Co-condensation reaction of triboronic acid and alkyl-functionalized tetraol resulting in COF-18 Å to 11 Å, reproduced with permission from ref. 77, copyright 2008 by John Wiley Sons, Inc., (b) general strategy for the pore surface engineering of COF-5 by a co-condensation of an azide bearing phenylboronic acid followed by click reaction. Reproduced with permission from ref. 78. Copyright 2011 Nature Publishing Group.

functionality need to be taken into account. Moreover, the anchoring group should not chemically interfere with the linkage motif of the COF synthesis. Nevertheless, the decoration of the pore walls of covalent organic frameworks with reactive organic functionalities enables a second modification step after the COF synthesis, a post synthetic modification (PSM). Nagai *et al.* introduced this pore surface engineering by using azide-decorated building blocks for the synthesis of different COFs.[78] In a post synthetic modification step, the azide moieties on the COF walls can react in a quantitative click-reaction with alkynes, thus forming triazole-linked groups on the pore surfaces. The authors could successfully show that it is possible to synthesize COF-5 and NiPc-COF with different amounts of azide-decorated phenylboronic acids (5%, 25%, 50%, 75%, 100%). X-ray powder diffraction patterns reveal that both scaffolds, hexagonal COF-5 and tetragonal NiPc-COF, remain unchanged by the introduction of azide groups into the framework walls. Reflection positions and linewidths are almost identical to those of the unfunctionalized COFs. The presence of the azide groups was spectroscopically proven with

IR measurements, revealing a strong vibrational mode at 2102 cm^{-1}. The azide-decorated COF-5 and NiPc-COF were reacted in a typical click-chemistry reaction with several alkyne-bearing groups, using a CuI catalyst (Fig. 7b). This way it was possible to tune the pore geometry and to customize the pore environment for a desired application, such as gas storage or separation. Decoration of the pore walls of COF-5 with acetyl groups resulted in a 16-fold increased selectivity of CO_2 over N_2 of 100%AcTrZ-COF-5 compared to ''naked'' COF-5.

The first internal functionalization of 3D COFs was achieved by Bunck *et al.* using a monomer truncation strategy.[79] The modification of COF-102[44] was realized by replacing one of the four boronic acid groups with a dodecyl-functionalization and a vinyl-functionalization (Fig. 8a). Co-condensation of the tetrahedral building block and the functionalized trigonal building block results in a modified COF-102-C_{12}/-allyl.

The functionalization was proven by IR spectroscopy of the powder and ^{1}H-NMR after digestion in CD_3CN/D_2O. The crystallinity of COF-102-C_{12}/-allyl was confirmed with X-ray diffraction. After staining the COF-102-allyl with OsO_4 vapor, transmission electron microscope images indicate a distribution of the allyl groups throughout the crystallites. These results show a homogeneous incorporation of the functionalized monomer into the lattice of the framework. In a subsequent study the truncated allyl groups inside the pores were used as anchor points for further organic post-modification reactions. The authors show that the framework can be successfully functionalized using a thiolene click reaction (Fig. 8b). The crystallinity and porosity of the framework remained intact after the modification reaction, illustrating the potential versatility of this reaction for other boronate ester-based COFs.[80]

1.2. COFs as electroactive materials

Theoretical insights. First theoretical studies based on the Density Functional Tight-Binding (DFTB) level investigated the structural, energetic and electronic properites of several existing and hypothetical two-dimensional COFs. The different stacking types, including AA, AB, serrated, and inclined and the resulting XRD patterns were calculated (see Fig. 9).[81] The theoretically obtained XRD patterns for the different stacking types often show similar peak positions and thus cannot be distinguished in the experimentally obtained patterns; however, differences in stacking energies were calculated. The authors found that all 2D COFs are semiconductors with band gaps between 1.7 eV and 4.0 eV, depending on the number of constituting aromatics and other factors. Importantly, the band gap was found to be

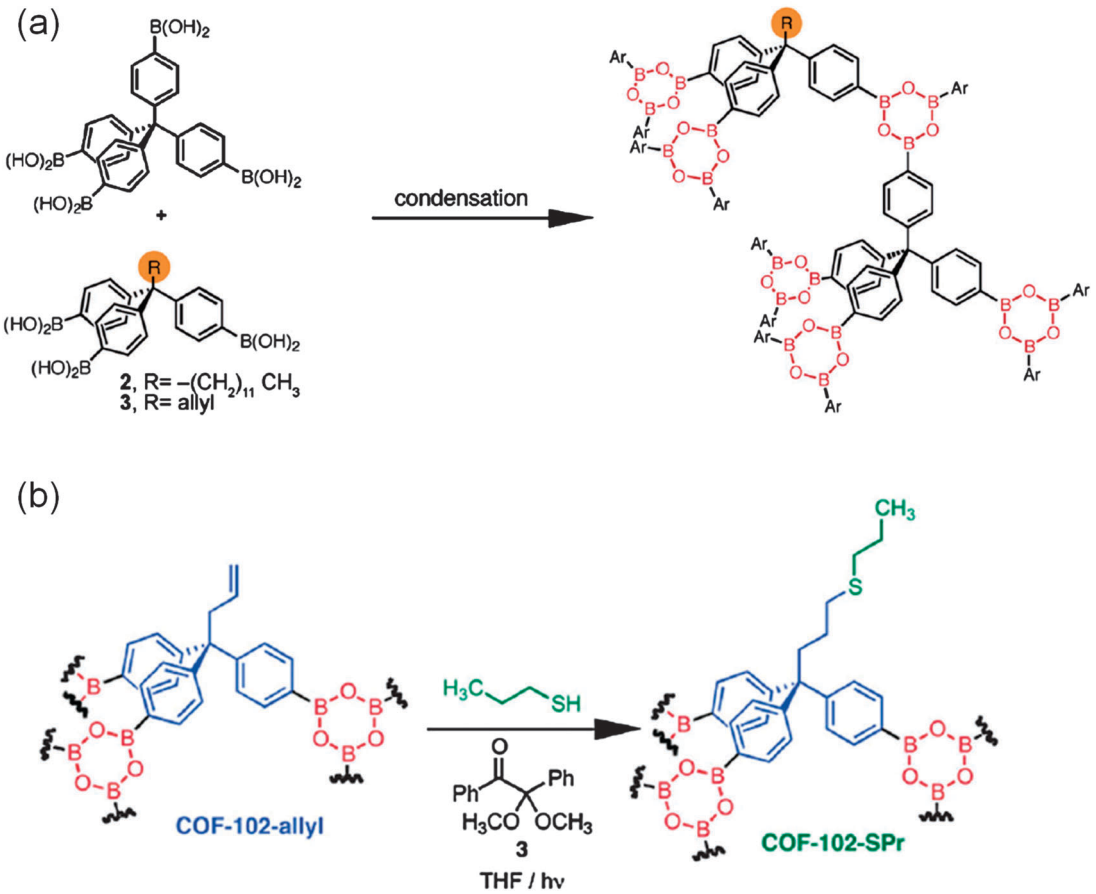

Fig. 8 (a) Co-condensation of a truncated linker and a tetraboronic acid results in the functionalized 3D COF-102, reproduced with permission from ref. 79, copyright 2012 by John Wiley Sons, Inc., (b) thiolene click reaction with COF-102/allyl results in COF-102-SPr, reproduced from ref. 80 with permission from The Royal Society of Chemistry.

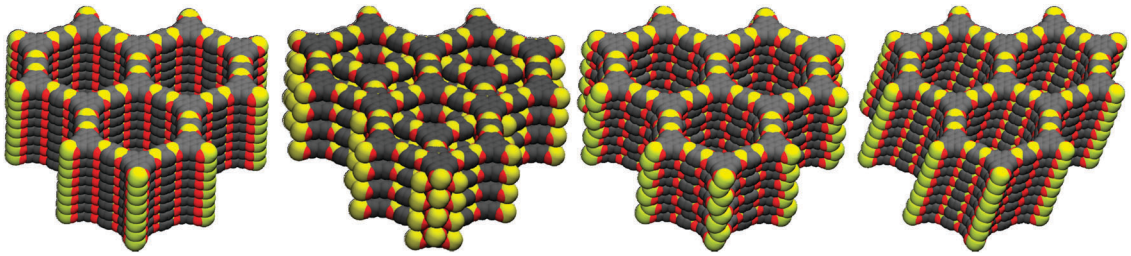

Fig. 9 Schematic representation of the different stacking types: AA, AB, serrated and inclined. Reproduced from ref. 81. Copyright 2010 Lukose *et al.*; licensee Beilstein-Institut.

strongly dependent on the stacking type and the distance between each COF layer. The hexagonal layers can stack in a armchair or zigzag conformation and for both the spatial layer offset was calculated to be around 0.14 nm. These conformations with a slight offset are stated to have less repulsive orbital interactions and thus are more stable than the widely accepted simple eclipsed stacking type.

Clancy and Dichtel used complementary density functional theory and molecular dynamics calculations to determine the interlayer distance in the diphenylbutadiyne (DPB)-based COF, DBP-HHTP COF. They suggest that in this material the adjacent layers are horizontally offset by about 0.17–0.18 nm rather than showing an eclipsed stacking, which agrees with the values reported by Heine.[81] Recently they extended the study to other boronate ester-based covalent organic frameworks. In all 33 cases of already synthesized structures and hypothetical structures an offset of 0.14–0.28 nm is predicted, thus the exact eclipsed stacking type for boronate-based COFs does not seem to be a realistic model.[82] This calculated offset in the stacking behavior might have a substantial impact on the charge carrier transport properties of COFs.[83,84]

The electronic characteristics of planar covalent organic frameworks on graphene were investigated by means of dispersion-corrected density functional theory.[85] The oriented growth of several hexagonal and square lattice COFs had already been shown by Dichtel and coworkers (see above).[86] Recently Gunasinghe *et al.* examined the self-assembly of two different COFs, the NiPc-PBBA and the HHTP-PBBA COF (PBBA is also called 1,4-benzenediboronic acid (BDBA) or phenyldiboronic acid (PDBA)), on graphene and the associated charge transfer at the interface (Fig. 10). Apparently, the self-assembly of COFs on graphene is aided by the strong delocalization of electrons from the graphene layer into the HOMO–LUMO levels of the COF, resulting in strong interactions between the orbitals.

Siebbeles *et al.* introduced a new computational method to calculate the extent of delocalization of charges in triphenylene-based

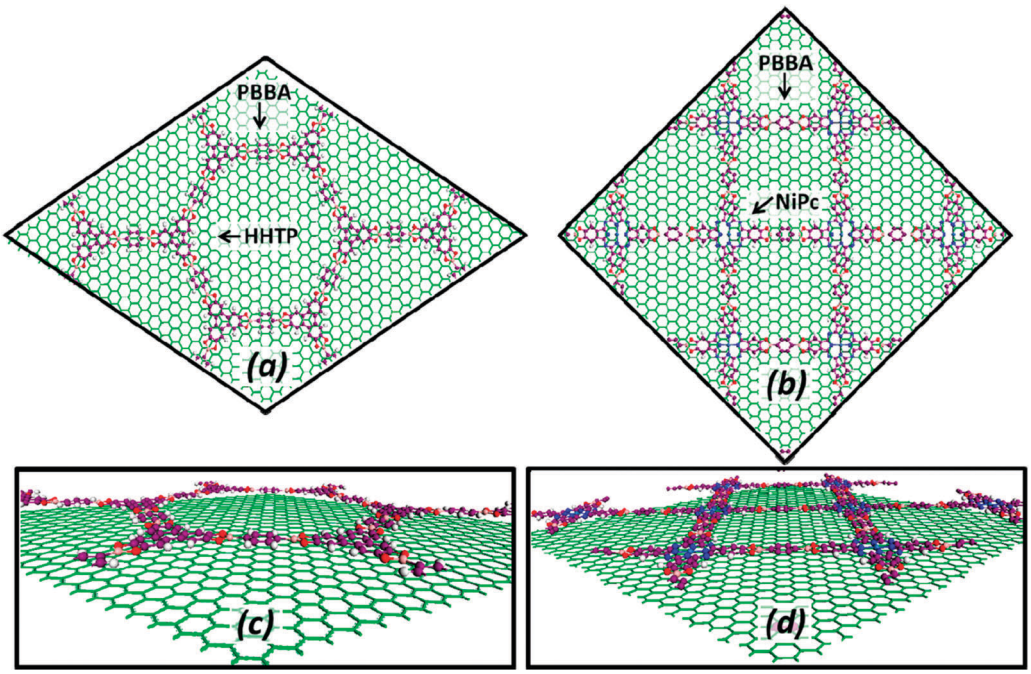

Fig. 10 Ball and stick models of (a) and (c) COF-5, and (b) and (d) NiPc-COF. Carbon atoms of COF are colored purple and of graphene green and hydrogen white, oxygen red, nitrogen blue, nickel light blue and boron pink, respectively. Reproduced with permission from ref. 85. Copyright 2012 American Chemical Society.

COFs with varied intermolecular distances and twist angles.[84] The authors found that the electronic coupling between the sheets is strongly dependent on the intermolecular distance and the twist angle, and suggested that the best electronic coupling will occur in ecliptically stacked COF sheets. Thus delocalized charges should be able to move *via* a temperature dependent band-like mechanism along the stacked columns and COF materials are expected to exhibit very high charge carrier mobilities. Experimental mobility studies at different temperatures will elucidate the charge transport mechanism. These calculations strongly motivate experimental investigations of the optoelectronic properties of these materials, and suggest that promising candidates for organic solar cells might be found in this family of materials.

Electroactive COFs. Recently Jiang and co-workers suggested that charge carriers can be transported along the framework of COFs.[87] They reported highly ordered conjugated pyrene-containing COFs. The co-condensation reaction of HHTP and pyrenediboronic acid (PDBA) results in the hexagonal crystalline framework, TP-COF (Fig. 11b), which exhibits open pores with a diameter of 3.14 nm and a specific surface area of 868 $m^2\ g^{-1}$. TP-COF exhibits semiconducting properties and blue luminescence. A blue luminescence has been previously reported for polyboronate.[88,89] Excitation at 376 nm or at 417 nm resulted in an emission at 474 nm, and excitation at 340 nm resulted in a strong emission at 376 nm from the pyrene units and a negligible weak emission at 402 nm from the triphenylene units, while a mere mixture of the starting materials displayed an emission at 402 nm. This was viewed as evidence for electronic coupling of the building blocks in the COF structure.

The electrical conductivity of TP-COF was measured using the two-probe method. For semiconducting materials a linear *I–V* curve is expected, this was observed for TP-COF under standard conditions, with a current of 4.3 nA at a bias voltage of 2 V between a 10 μm gap. The COF was dispersed in acetone and drop-cast on the electrode, the second electrode was then thermally evaporated on the COF film. Upon doping the framework with iodine a significant rise in current up to 20 nA was observed, thus suggesting a p-type semiconducting character of TP-COF. Self-condensation of pyrenediboronic acid (Fig. 11a) also results in an optoelectronically active framework with a pore size of 1.73 nm and a specific surface area of 923 $m^2\ g^{-1}$.

Ppy-COF generates a moderate photocurrent of 5 nA upon illumination with a xenon lamp, which was attributed to the defined conduction paths for charge migration provided through the highly ordered structure.[90] For the device fabrication for photoconductivity measurements, the COF was dispersed in PMMA (Ppy-COF/PMMA = 50/50 wt%), the resulting film thickness was 100 μm. Another photoconductive COF with a tetragonal metallophthalocyanine building block, NiPc-COF (Fig. 11c), was reported to have high charge carrier mobilities.[51] Incorporating phthalocyanine into the framework broadens the optical absorption profile of the COF. The eclipsed stacking of the phthalocyanine and arene boronic acid leads to an open framework with a surface area of 624 $m^2\ g^{-1}$ and a micropore diameter of 1.9 nm. Upon irradiation with a xenon lamp the current at 1 V

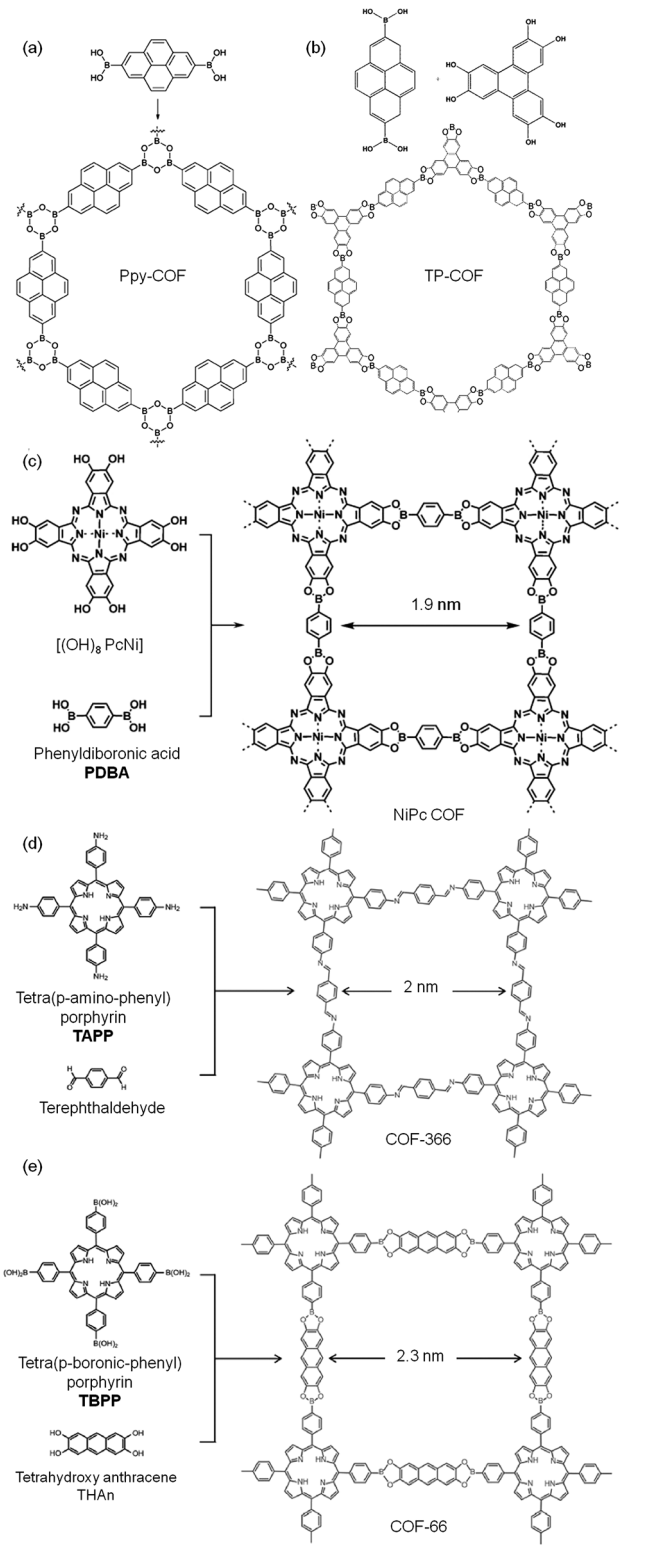

Fig. 11 (a) Ppy-COF synthesized by self-condensation of pyrene diboronic acid, (b) TP-COF synthesized by a co-condensation reaction of pyrenediboronic acid and hexahydroxytriphenylene. Tetragonal COFs with reported high charge carrier mobility: (c) nickel phthalocyanine-based COF, reproduced with permission from ref. 51, copyright 2011 by John Wiley Sons, Inc., (d) porphyrin-based tetragonal COFs synthesized by imine condensation and (e) by boronate ester condensation reactions. Reproduced with permission from ref. 54. Copyright 2011 American Chemical Society.

bias increased from 20 nA to 3 μA, furthermore panchromatic photoresponse was very fast and reproducible without deterioration. The intrinsic charge carrier mobility of NiPc-COF and the following structures shown in this review were obtained with laser flash-photolysis time-resolved microwave conductivity measurements (FP-TRMC), which give the product $\phi^*\Sigma\mu$ (ϕ is the photocarrier generation yield and $\Sigma\mu$ is the sum of the charge carrier mobilities). The yield of photocarrier generation ϕ was determined by integration of the time-of-flight (TOF) transients at different bias voltages. The number of charge carriers was extrapolated to a bias of 0 V, leading to the charge carrier generation yield ϕ, expressed as the number of charge carriers per photon. Yaghi extended the scope of macrocyclic COFs exhibiting semiconductor properties with two new structures based on the condensation reactions of porphyrin derivatives (Fig. 11d and e), through either boronate ester formation with tetrahydroxyanthracene (COF-66) or imine bond formation with terephthalaldehyde (COF-366), respectively.[54] With time-resolved microwave conductivity measurements of a 1.5 μm thick COF/poly(methylmethacrylate) (60 : 40 wt%) film sandwiched between indium tin oxide and aluminum electrodes, the hole mobilities of COF-66 and COF-366 were reported to be as high as 3.0 $cm^2\ V^{-1}\ s^{-1}$ and 8.1 $cm^2\ V^{-1}\ s^{-1}$, respectively.

The first electron-transporting COF was created by substituting the benzene groups at the edges of the NiPc-COF with electron-deficient benzothiadiazole (BTDA) building blocks (Fig. 12a). The resulting n-channel NiPc-BTDA COF was reported to exhibit a high electron mobility of 0.6 $cm^2\ V^{-1}\ s^{-1}$. The absorbance of this COF is very broad and ranges up to 1000 nm, resulting in a panchromatic photoresponse with high sensitivity to near-infrared photons. Upon excitation with white light photocurrent at 1 V bias was enhanced from 250 nA to 15 μA (Fig. 12a).[55]

Semiconducting COFs with tunable charge carrier transport behavior were created with 2D porphyrin COFs having different central metals (MP-COFs).[91] Insertion of a copper central metal leads to electron transport along the framework, whereas free base porphyrin COF is hole conducting. The zincated material ZnP-COF exhibits ambipolar charge transport. Flash-photolysis time-resolved microwave conductivity (FP/TRMC) methods under argon atmosphere gave the total carrier mobilities (electrons and holes), while in measurements under an SF_6 atmosphere the electrons are trapped, hence giving only hole mobilities. Another example of ambipolar charge transport, a 2D D–A-COF, was formed by a co-condensation reaction of a benzothiadiazole bearing boronic acid with the triangular building block HHTP.[92] The resulting COF with a pore size of about 2.8 nm was reported to exhibit high electron and hole mobilities of 0.04 and 0.01 $cm^2\ V^{-1}\ s^{-1}$, respectively. In the case of D–A-COF it was suggested that the electrons can be conducted along the columns of the benzothiadiazole unit and the holes along the HHTP columns (Fig. 12b).

Control over morphology and the creation of separated domains of donor and acceptor phases is one of the challenges in creating efficient organic solar cells. One possibility to gain control over the location of the donor and the acceptor at an atomistic level is the incorporation of D and A molecules into the crystalline structure of a covalent organic framework. Jiang and coworkers reported that by co-condensing the electron-accepting benzothiadiazole benzenediboronic acid and the donor hexahydroxytriphenylene, a D–A-heterojunction with atomistically separated periodic D columns and A columns can be synthesized.[92] This 'ambipolar' COF shows a high on–off ratio photoconductive response and high charge carrier mobilities. The charge carrier dynamics of these D–A-COFs were elucidated with time-resolved spectroscopy. The generation of free charges upon light absorption in the D–A columns is achieved within 2 ps. The π-stacking of the COF allows for delocalization of the charges and suppresses recombination. Expanding on the intracrystalline D–A theme, a COF based on zinc phthalocyanine serving as the donor and naphthalene diimide (NDI) as the acceptor shows light absorption over a wide range of the visible spectrum and into the near IR up to 1100 nm (see Fig. 12c).[53,93] Differential pulse voltammetric measurements of the built-in D–A system showed oxidation of the ZnPc at 0.42 eV and a reduction of the NDI at −0.52 V, which the authors interpreted as a large exothermic driving force for electron transfer. The electrochemical measurements were recorded with a dispersion of ZnPc-NDI-COF in benzonitrile, with respect to a $Ag/AgNO_3$ reference electrode. The ultrafast charge separation and the long retention of the charge separated state, due to the delocalization along the π-columns in the D–A-COF, illustrate the high potential of these systems for photovoltaic applications.

The familiy of semiconducting COFs is constantly growing. Recently Bertrand *et al.* reported three new thiophene-based covalent organic frameworks (Fig. 13a). In general the boronic acid equipped thiophene building blocks allow COF formation, following the concepts of reticular chemistry.[94] However, bent monomers such as the thiophene diboronic acid tend to form defects in the structure, due to their nonlinear binding motif. Combining two thiophene molecules in an antiparallel fashion leads to a linear linkage motif and COF structures can be readily obtained with high crystallinity. The authors could also show the formation of a charge transfer complex between the thiophene diboronic acid building block and tetracyanoquinodimethane (TCNQ), while electron transfer from the COF to the TCNQ was not observed. Other oxidizing agents such as 2,3-dichloro-5,6-dicyano-1,4-benzoquinone (DDQ), chloranyl or I_2 caused degradation of the framework. These results illustrate the importance of a careful search for suitable redox partners to achieve full electron transfer without disrupting the crystalline framework.

We could recently show that it is possible to integrate covalent organic frameworks in a bulk-heterojunction photovoltaic cell.[95] The thienothiophene-based TT-COF was synthesized in a co-condensation reaction of thienothiophene diboronic acid with HHTP. Upon irradiation with light the system showed significant photocurrent. The large surface area of 1800 $m^2\ g^{-1}$ and the 3 nm open pores of the hole-transporting TT-COF enable the uptake of large electron transporting materials, such as the fullerene derivative PCBM (see Fig. 13b). Inclusion of PCBM leads to a novel periodic interpenetrated donor–acceptor

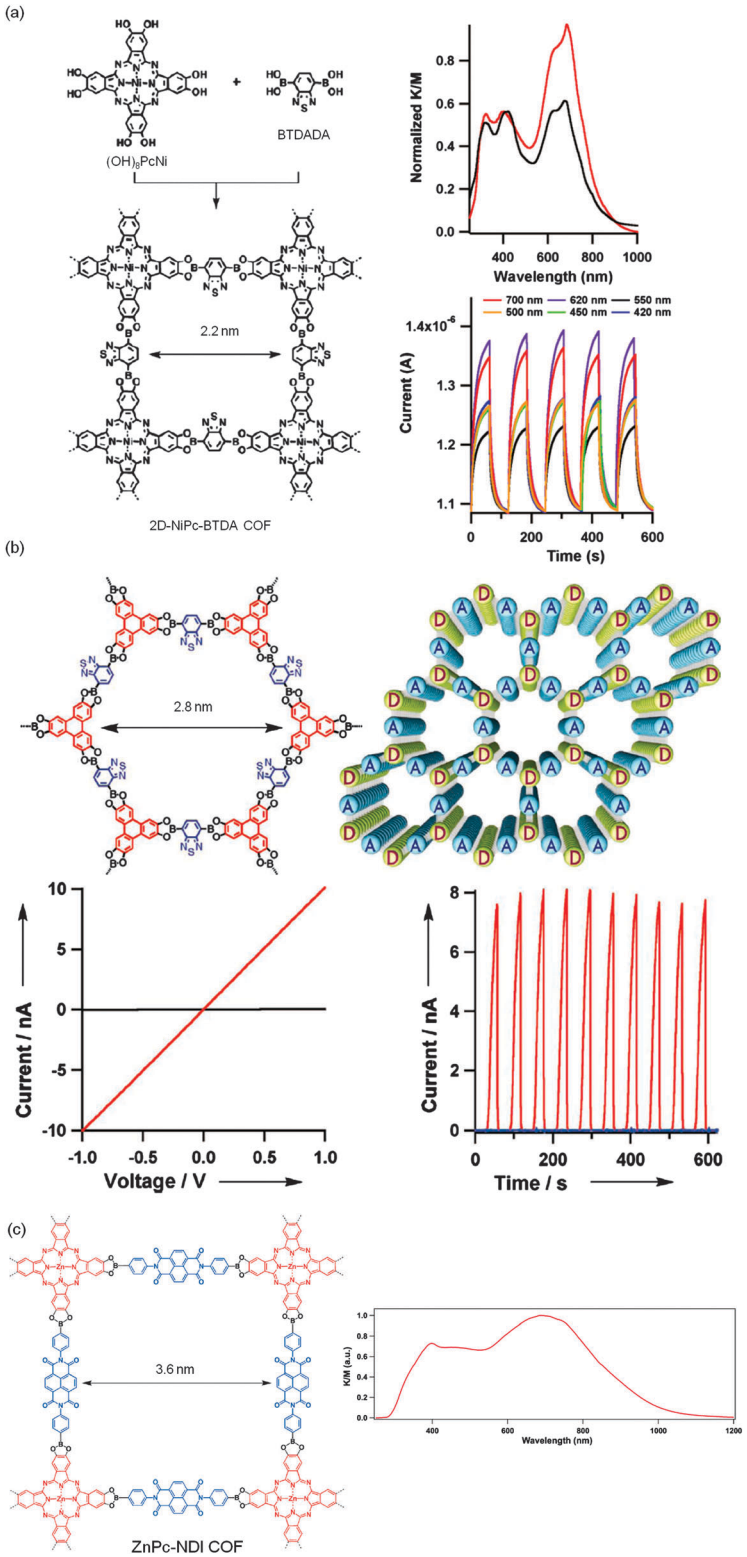

Fig. 12 (a) Schematic synthesis pathway for NiPc-BTDA with absorbance spectra of 2D-NiPc-BTDA COF (red) and $(MeO)_8PcNi$ (black), and on–off switching of photocurrent of 2D-NiPc-BTDA COF under the bias voltage of 1.0 V at different wavelengths, reproduced with permission from ref. 55, copyright 2011 American Chemical Society, (b) D–A-COF co-condensed from benzothiadiazole diboronic acid and HHTP shows no current in the dark (left, black) and a linear photoresponse upon irradiation (red) with visible light from a xenon light source, and exhibits a high on–off ratio photoconductive response (right), reproduced with permission from ref. 92, copyright 2012 by John Wiley Sons, Inc., (c) schematic representation of the structure of ZnPc-NDI COF with the absorbance spectrum, reproduced with permission from ref. 93. Copyright 2013 by John Wiley Sons, Inc.

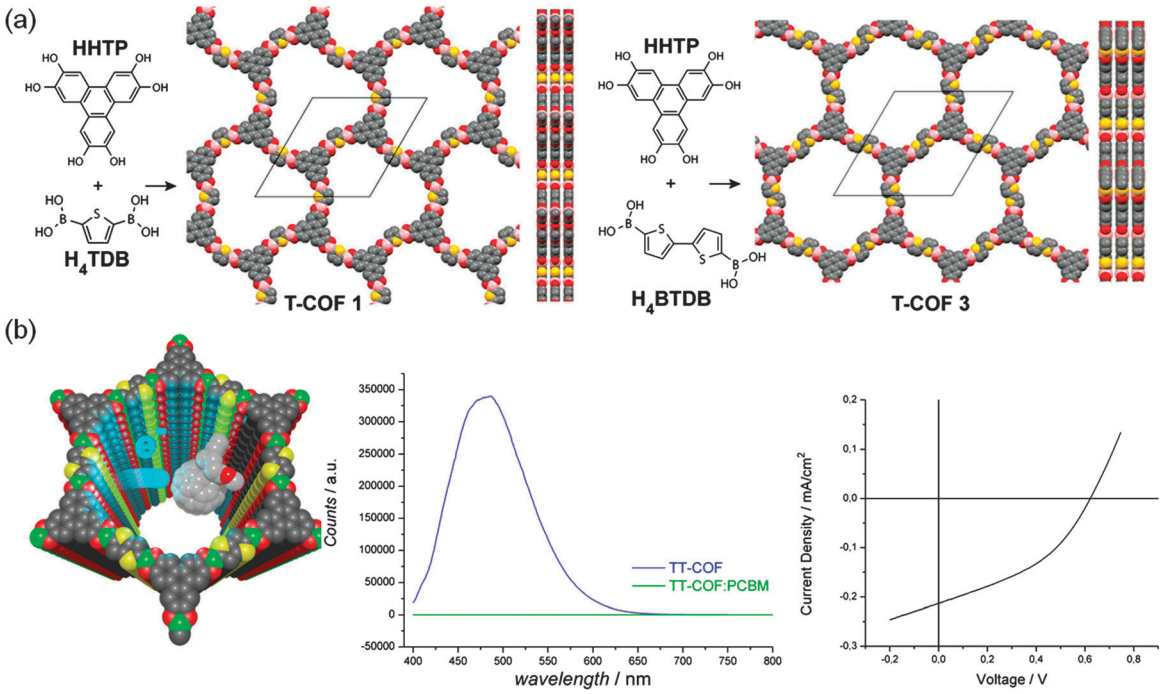

Fig. 13 (a) Schematic representation of T-COF 1 (left) and T-COF-3 based on thiophene-based building blocks, reproduced with permission from ref. 94, copyright 2013 by the National Academy of Sciences of the United States of America, (b) thienothiophene-based TT-COF showing charge transfer to included PCBM as indicated by complete photoluminescence quenching, right: *I*–*V*-profile of the first COF-based photovoltaic device, reproduced with permission from ref. 95. Copyright 2013 by John Wiley Sons, Inc.

system, which shows the spectroscopic signatures of efficient charge transfer at the nanoscale and can act as a photovoltaic cell.

Summary and perspective

The discovery of the family of covalent organic frameworks heralds a new age in the design of crystalline porous materials. The reticular synthesis approach of combining rigid organic building blocks and the unique intrinsic properties of these materials promise access to numerous possible applications. Although the research field is still in its infancy, several powerful synthesis strategies and the resulting COFs have already been demonstrated, illustrating the great potential of this family of materials. The development of additional new synthetic strategies and new linkage systems will provide access to new members with novel functionalities in the COF family.

One important aspect in designing novel 2D COFs relates to the exact stacking motif of the building blocks; control of the stacking is expected to have a profound effect on optoelectronic properties. The interplay between theoretical investigations and synthetic realization of stacking motifs with subtle structural differences is anticipated to shed more light on this important feature of COFs. Moreover, the degree of lateral conjugation and electronic coupling in 2D COFs, together with control over domain size and crystal morphology will be additional means to modify and optimize the behavior of excitons and charge carriers in these systems. A further extension of these concepts may be realized by chemical functionalization of the walls of the COFs. This approach as well as refilling the pore system with complementary donor or acceptor phases rests on the ability to clean the pores from residues resulting from the synthesis – careful optimization of extraction techniques will be important.

There will also be a need to enhance the chemical stability of COFs for some applications. This can be achieved by using new building blocks and new linkage motifs. As discussed above, one novel approach is the formation of imine-linked networks that can undergo keto–enol tautomerism to yield COFs that are stable in boiling water, acids and bases.

With judicious use and further development of the above synthetic tools, the physical and chemical properties, such as thermal stability, absorbance spectrum and conductivity of COFs can be tailored by the choice of the appropriate building blocks. The well-defined crystalline structure and the large accessible internal surface area and porosity, which can be filled with sizeable functional molecules, point to the great potential of these materials as excellent model systems for investigating ordered and interpenetrated networks of donor–acceptor systems at the nanoscale.

Acknowledgements

The authors are grateful for funding from the German Science Foundation (DFG; Research Cluster NIM) and the Free State of Bavaria (Research Network SolTech). The research leading to these results has received funding from the European Research Council under the European Union's Seventh Framework Programme (FP7/2007-2013)/ERC grant agreement no. 321339.

References

1 C. J. Rhodes, *Annu. Rep. Prog. Chem., Sect. C: Phys. Chem.*, 2007, **103**, 287–325.
2 K. Moller and T. Bein, *Chem. Soc. Rev.*, 2013, **42**, 3689–3707.
3 N. Stock and S. Biswas, *Chem. Rev.*, 2011, **112**, 933–969.
4 X. Feng, X. Ding and D. Jiang, *Chem. Soc. Rev.*, 2012, **41**, 6010–6022.
5 S.-Y. Ding and W. Wang, *Chem. Soc. Rev.*, 2013, **42**, 548–568.
6 W. Li, Q. Yue, Y. Deng and D. Zhao, *Adv. Mater.*, 2013, **25**, 5129–5152.
7 H.-C. Zhou, J. R. Long and O. M. Yaghi, *Chem. Rev.*, 2012, **112**, 673–674.
8 K.-S. Liao, S. D. Yambem, A. Haldar, N. J. Alley and S. A. Curran, *Energies*, 2010, **3**, 1212–1250.
9 G. Li, R. Zhu and Y. Yang, *Nat. Photonics*, 2012, **6**, 153–161.
10 H. Hoppe and N. S. Sariciftci, *J. Mater. Res.*, 2004, **19**, 1924–1945.
11 C. W. Tang, *Appl. Phys. Lett.*, 1986, **48**, 183–185.
12 J. C. Hummelen, B. W. Knight, F. LePeq, F. Wudl, J. Yao and C. L. Wilkins, *J. Org. Chem.*, 1995, **60**, 532–538.
13 N. S. Sariciftci, L. Smilowitz, A. J. Heeger and F. Wudl, *Science*, 1992, **258**, 1474–1476.
14 S. Morita, A. A. Zakhidov and K. Yoshino, *Solid State Commun.*, 1992, **82**, 249–252.
15 N. S. Sariciftci, L. Smilowitz, A. J. Heeger and F. Wudl, *Synth. Met.*, 1993, **59**, 333–352.
16 G. Yu, J. Gao, J. C. Hummelen, F. Wudl and A. J. Heeger, *Science*, 1995, **270**, 1789–1791.
17 J. J. M. Halls, C. A. Walsh, N. C. Greenham, E. A. Marseglia, R. H. Friend, S. C. Moratti and A. B. Holmes, *Nature*, 1995, **376**, 498–500.
18 W. Ma, C. Yang, X. Gong, K. Lee and A. J. Heeger, *Adv. Funct. Mater.*, 2005, **15**, 1617–1622.
19 G. Li, V. Shrotriya, J. Huang, Y. Yao, T. Moriarty, K. Emery and Y. Yang, *Nat. Mater.*, 2005, **4**, 864–868.
20 M. T. Dang, L. Hirsch and G. Wantz, *Adv. Mater.*, 2011, **23**, 3597–3602.
21 M. T. Dang, L. Hirsch, G. Wantz and J. D. Wuest, *Chem. Rev.*, 2013, **113**, 3734–3765.
22 A. J. Moulé and K. Meerholz, *Adv. Mater.*, 2008, **20**, 240–245.
23 X. Yang, J. Loos, S. C. Veenstra, W. J. H. Verhees, M. M. Wienk, J. M. Kroon, M. A. J. Michels and R. A. J. Janssen, *Nano Lett.*, 2005, **5**, 579–583.
24 T. Benincori, E. Brenna, F. Sannicolò, L. Trimarco, G. Zotti and P. Sozzani, *Angew. Chem.*, 1996, **108**, 718–720.
25 A. Yassar, M. Hmyene, D. C. Loveday and J. P. Ferraris, *Synth. Met.*, 1997, **84**, 231–232.
26 A. M. Ramos, M. T. Rispens, J. K. J. van Duren, J. C. Hummelen and R. A. J. Janssen, *J. Am. Chem. Soc.*, 2001, **123**, 6714–6715.
27 F. Zhang, M. Svensson, M. R. Andersson, M. Maggini, S. Bucella, E. Menna and O. Inganäs, *Adv. Mater.*, 2001, **13**, 1871–1874.
28 A. Cravino, G. Zerza, M. Maggini, S. Bucella, M. Svensson, M. R. Andersson, H. Neugebauer, C. J. Brabec and N. S. Sariciftci, *Monatsh. Chem.*, 2003, **134**, 519–527.
29 U. Stalmach, B. de Boer, C. Videlot, P. F. van Hutten and G. Hadziioannou, *J. Am. Chem. Soc.*, 2000, **122**, 5464–5472.
30 R. A. Segalman, B. McCulloch, S. Kirmayer and J. J. Urban, *Macromolecules*, 2009, **42**, 9205–9216.
31 S.-S. Sun, *Sol. Energy Mater.*, 2003, **79**, 257–264.
32 C. Park, J. Yoon and E. L. Thomas, *Polymer*, 2003, **44**, 6725–6760.
33 D. Venkataraman, S. Yurt, B. H. Venkatraman and N. Gavvalapalli, *J. Phys. Chem. Lett.*, 2010, **1**, 947–958.
34 S. M. Lindner and M. Thelakkat, *Macromolecules*, 2004, **37**, 8832–8835.
35 M. Sommer, S. M. Lindner and M. Thelakkat, *Adv. Funct. Mater.*, 2007, **17**, 1493–1500.
36 N. Sary, F. Richard, C. Brochon, N. Leclerc, P. Lévêque, J.-N. Audinot, S. Berson, T. Heiser, G. Hadziioannou and R. Mezzenga, *Adv. Mater.*, 2010, **22**, 763–768.
37 J. Weickert, R. B. Dunbar, H. C. Hesse, W. Wiedemann and L. Schmidt-Mende, *Adv. Mater.*, 2011, **23**, 1810–1828.
38 L. Schmidt-Mende, A. Fechtenkötter, K. Müllen, E. Moons, R. H. Friend and J. D. MacKenzie, *Science*, 2001, **293**, 1119–1122.
39 Y. Yang, K. Mielczarek, M. Aryal, A. Zakhidov and W. Hu, *ACS Nano*, 2012, **6**, 2877–2892.
40 I. Botiz and S. B. Darling, *Mater. Today*, 2010, **13**, 42–51.
41 M. D. McGehee, *MRS Bull.*, 2009, **34**, 95–100.
42 T. Dittrich, A. Belaidi and A. Ennaoui, *Sol. Energy Mater.*, 2011, **95**, 1527–1536.
43 A. P. Côté, A. I. Benin, N. W. Ockwig, M. O'Keeffe, A. J. Matzger and O. M. Yaghi, *Science*, 2005, **310**, 1166–1170.
44 H. M. El-Kaderi, J. R. Hunt, J. L. Mendoza-Cortés, A. P. Côté, R. E. Taylor, M. O'Keeffe and O. M. Yaghi, *Science*, 2007, **316**, 268–272.
45 D. G. Hall, *Boronic Acids*, Wiley-VCH, Weinheim, 2005.
46 R. W. Tilford, W. R. Gemmill, H.-C. zur Loye and J. J. Lavigne, *Chem. Mater.*, 2006, **18**, 5296–5301.
47 A. P. Cote, H. M. El-Kaderi, H. Furukawa, J. R. Hunt and O. M. Yaghi, *J. Am. Chem. Soc.*, 2007, **129**, 12914–12915.
48 M. Dogru, A. Sonnauer, A. Gavryushin, P. Knochel and T. Bein, *Chem. Commun.*, 2011, **47**, 1707–1709.
49 E. L. Spitler, B. T. Koo, J. L. Novotney, J. W. Colson, F. J. Uribe-Romo, G. D. Gutierrez, P. Clancy and W. R. Dichtel, *J. Am. Chem. Soc.*, 2011, **133**, 19416–19421.
50 E. L. Spitler and W. R. Dichtel, *Nat. Chem.*, 2010, **2**, 672–677.
51 X. Ding, J. Guo, X. Feng, Y. Honsho, J. Guo, S. Seki, P. Maitarad, A. Saeki, S. Nagase and D. Jiang, *Angew. Chem., Int. Ed.*, 2011, **50**, 1289–1293.
52 X. Feng, L. Chen, Y. Dong and D. Jiang, *Chem. Commun.*, 2011, **47**, 1979–1981.
53 E. L. Spitler, J. W. Colson, F. J. Uribe-Romo, A. R. Woll, M. R. Giovino, A. Saldivar and W. R. Dichtel, *Angew. Chem., Int. Ed.*, 2012, **51**, 2623–2627.
54 S. Wan, F. Gandara, A. Asano, H. Furukawa, A. Saeki, S. K. Dey, L. Liao, M. W. Ambrogio, Y. Y. Botros, X. Duan, S. Seki, J. F. Stoddart and O. M. Yaghi, *Chem. Mater.*, 2011, **23**, 4094–4097.
55 X. Ding, L. Chen, Y. Honsho, X. Feng, O. Saengsawang, J. Guo, A. Saeki, S. Seki, S. Irle, S. Nagase, V. Parasuk and D. Jiang, *J. Am. Chem. Soc.*, 2011, **133**, 14510–14513.
56 N. L. Campbell, R. Clowes, L. K. Ritchie and A. I. Cooper, *Chem. Mater.*, 2009, **21**, 204–206.
57 M. Dogru, A. Sonnauer, S. Zimdars, M. Doblinger, P. Knochel and T. Bein, *CrystEngComm*, 2013, **15**, 1500–1502.
58 S.-T. Yang, J. Kim, H.-Y. Cho, S. Kim and W.-S. Ahn, *RSC Adv.*, 2012, **2**, 10179–10181.
59 S. Kandambeth, A. Mallick, B. Lukose, M. V. Mane, T. Heine and R. Banerjee, *J. Am. Chem. Soc.*, 2012, **134**, 19524–19527.
60 B. P. Biswal, S. Chandra, S. Kandambeth, B. Lukose, T. Heine and R. Banerjee, *J. Am. Chem. Soc.*, 2013, **135**, 5328–5331.
61 R. Hunt Joseph, J. Doonan Christian, D. LeVangie James, P. Cote Adrien and M. Yaghi Omar, *J. Am. Chem. Soc.*, 2008, **130**, 11872–11873.
62 H. K. Chae, D. Y. Siberio-Perez, J. Kim, Y. Go, M. Eddaoudi, A. J. Matzger, M. O'Keeffe and O. M. Yaghi, *Nature*, 2004, **427**, 523–527.
63 G. Ferey, C. Mellot-Draznieks, C. Serre, F. Millange, J. Dutour, S. Surble and I. Margiolaki, *Science*, 2005, **309**, 2040–2042.
64 H. Furukawa and O. M. Yaghi, *J. Am. Chem. Soc.*, 2009, **131**, 8875–8883.
65 S. S. Han, H. Furukawa, O. M. Yaghi and W. A. Goddard III, *J. Am. Chem. Soc.*, 2008, **130**, 11580–11581.
66 C. J. Doonan, D. J. Tranchemontagne, T. G. Glover, J. R. Hunt and O. M. Yaghi, *Nat. Chem.*, 2010, **2**, 235–238.
67 J. L. Mendoza-Cortes, S. S. Han, H. Furukawa, O. M. Yaghi and W. A. Goddard, *J. Phys. Chem. A*, 2010, **114**, 10824–10833.
68 J. L. Mendoza-Cortes, T. A. Pascal and W. A. Goddard, *J. Phys. Chem. A*, 2011, **115**, 13852–13857.
69 E. Tylianakis, E. Klontzas and G. E. Froudakis, *Nanoscale*, 2011, **3**, 856–869.
70 E. Klontzas, E. Tylianakis and G. E. Froudakis, *J. Phys. Chem. C*, 2008, **112**, 9095–9098.
71 F. J. Uribe-Romo, J. R. Hunt, H. Furukawa, C. Klöck, M. O'Keeffe and O. M. Yaghi, *J. Am. Chem. Soc.*, 2009, **131**, 4570–4571.
72 S.-Y. Ding, J. Gao, Q. Wang, Y. Zhang, W.-G. Song, C.-Y. Su and W. Wang, *J. Am. Chem. Soc.*, 2011, **133**, 19816–19822.
73 M. G. Rabbani, A. K. Sekizkardes, Z. Kahveci, T. E. Reich, R. Ding and H. M. El-Kaderi, *Chem.–Eur. J.*, 2013, **19**, 3324–3328.
74 F. J. Uribe-Romo, C. J. Doonan, H. Furukawa, K. Oisaki and O. M. Yaghi, *J. Am. Chem. Soc.*, 2011, **133**, 11478–11481.

75 K. T. Jackson, T. E. Reich and H. M. El-Kaderi, *Chem. Commun.*, 2012, **48**, 8823–8825.
76 P. Kuhn, M. Antonietti and A. Thomas, *Angew. Chem., Int. Ed.*, 2008, **47**, 3450–3453.
77 R. W. Tilford, S. J. Mugavero III, P. J. Pellechia and J. J. Lavigne, *Adv. Mater.*, 2008, **20**, 2741–2746.
78 A. Nagai, Z. Guo, X. Feng, S. Jin, X. Chen, X. Ding and D. Jiang, *Nat. Commun.*, 2011, **2**, 536.
79 D. N. Bunck and W. R. Dichtel, *Angew. Chem., Int. Ed.*, 2012, **51**, 1885–1889.
80 D. N. Bunck and W. R. Dichtel, *Chem. Commun.*, 2013, **49**, 2457–2459.
81 B. Lukose, A. Kuc, J. Frenzel and T. Heine, *Beilstein J. Nanotechnol.*, 2010, **1**, 60–70.
82 B. T. Koo, W. R. Dichtel and P. Clancy, *J. Mater. Chem.*, 2012, **22**, 17460–17469.
83 V. Coropceanu, J. Cornil, D. A. da Silva Filho, Y. Olivier, R. Silbey and J.-L. Brédas, *Chem. Rev.*, 2007, **107**, 926–952.
84 S. Patwardhan, A. A. Kocherzhenko, F. C. Grozema and L. D. A. Siebbeles, *J. Phys. Chem. C*, 2011, **115**, 11768–11772.
85 R. N. Gunasinghe, D. G. Reuven, K. Suggs and X.-Q. Wang, *J. Phys. Chem. Lett.*, 2012, **3**, 3048–3052.
86 J. W. Colson, A. R. Woll, A. Mukherjee, M. P. Levendorf, E. L. Spitler, V. B. Shields, M. G. Spencer, J. Park and W. R. Dichtel, *Science*, 2011, **332**, 228–231.
87 S. Wan, J. Guo, J. Kim, H. Ihee and D. Jiang, *Angew. Chem.*, 2009, **121**, 3253.
88 W. Niu, M. D. Smith and J. J. Lavigne, *J. Am. Chem. Soc.*, 2006, **128**, 16466–16467.
89 Y. Li, J. Ding, M. Day, Y. Tao, J. Lu and M. D'Iorio, *Chem. Mater.*, 2003, **15**, 4936–4943.
90 S. Wan, J. Guo, J. Kim, H. Ihee and D. Jiang, *Angew. Chem., Int. Ed.*, 2009, **48**, 5439–5442.
91 X. Feng, L. Liu, Y. Honsho, A. Saeki, S. Seki, S. Irle, Y. Dong, A. Nagai and D. Jiang, *Angew. Chem., Int. Ed.*, 2012, **51**, 2618–2622.
92 X. Feng, L. Chen, Y. Honsho, O. Saengsawang, L. Liu, L. Wang, A. Saeki, S. Irle, S. Seki, Y. Dong and D. Jiang, *Adv. Mater.*, 2012, **24**, 3026–3031.
93 S. Jin, X. Ding, X. Feng, M. Supur, K. Furukawa, S. Takahashi, M. Addicoat, M. E. El-Khouly, T. Nakamura, S. Irle, S. Fukuzumi, A. Nagai and D. Jiang, *Angew. Chem., Int. Ed.*, 2013, **52**, 2017–2021.
94 G. H. V. Bertrand, V. K. Michaelis, T.-C. Ong, R. G. Griffin and M. Dincă, *Proc. Natl. Acad. Sci. U. S. A.*, 2013, **110**, 4923–4928.
95 M. Dogru, M. Handloser, F. Auras, T. Kunz, D. Medina, A. Hartschuh, P. Knochel and T. Bein, *Angew. Chem.*, 2013, **125**, 2992–2996.

